Building Tomorrow's Society
Bâtir la Société de Demain

Fredericton, Canada
June 13 – June 16, 2018/ *Juin 13 – Juin 16, 2018*

DEBRIS DAMMING LOADS AND EFFECT IN TSUNAMI-LIKE EVENTS

Stolle, Jacob[1,5], Nistor, Ioan[1], Takabatake, Tomoyuki[2], Goseberg, Nils[3], Petriu, Emil[4], Shibayama, Tomoya[2]
[1] Department of Civil Engineering, University of Ottawa, Canada
[2] Department of Civil and Environmental Engineering, Waseda University, Japan
[3] Leichtweiß-Institute for Hydraulic Engineering and Water Resources, Technische Universität Braunschweig, Germany
[4] School of Electrical Engineering and Computer Science, University of Ottawa, Canada
[5] jstol065@uottawa.ca

Abstract: Debris loading during extreme flooding events has been documented by many post-tsunami field surveys of disaster-stricken communities and, as such, it is now considered and accounted for as a critical design consideration in building resilient infrastructure. Debris damming is one of the debris loads of concern, occurring when solid objects entrained within the inundating flow accumulate at the face of a structure or a structural element. The presence of the debris dam results in increased drag loads on the structure and can have other associated effects, such as flow runup and flow accelerations, that can cause increased scouring at foundations. The focus of debris damming studies has been within river engineering: therefore, previous studies have been performed in steady-state conditions. The study presented here is the first to examine debris damming in transient, supercritical flow conditions. The study uses a modified dam-break wave as the hydrodynamic forcing condition and the debris are scaled down debris types common in coastal areas (shipping containers, hydro poles, and boards). The study qualitatively examines the difference in the debris damming mechanisms as a result of distinct flow conditions associated with a dam-break wave interacting with a surface-piercing obstacle. Additionally, the study aimed to determine the influence of the debris dam. It was found that maximum loading condition occurred earlier and of greater magnitude than for the clear water case.

1 INTRODUCTION

The recent devastation generated by major flooding events, such as the 2004 Indian Ocean Tsunami, captured the attention of regulatory agencies and research bodies worldwide due to the failure of coastal structures and critical infrastructure that had been designed to withstand these events (Yeh et al., 2013). One of the primary explanations for these failures was that building standards and design codes did not properly address the variety of extreme loads associated with a tsunami event (Esteban et al., 2015; Yeh et al., 2014). To address this concern in North America, particularly along the West Coast, where the region is at-risk of earthquakes along the Cascadia subduction zone (CREW, 2013), the American Society of Civil Engineering (ASCE) has developed a chapter (ASCE7 Chapter 6) around the design of critical infrastructure exposed to tsunami events (Chock, 2016).

Debris loading was identified within the standard as one of the critical loads. On the one hand, debris impact is of major concern for short-period high-strength forces on structures (Nistor et al. 2017). One the other hand, debris damming occurs when waterborne debris accumulates at the face of a structure or in between adjacent structures. This accumulation can obstruct openings in buildings where water previously could

flow freely. The obstruction results in changing hydrostatic and hydrodynamic loads exerted on the structures.

Within standards worldwide, debris damming loads are generally accounted for as hydrodynamic loads acting on a structure (FEMA, 2012; CSA, 2006; AASHTO, 2012), using the drag equation (Bremm et al., 2015):

[1] $F_D = \frac{1}{2} C_D \rho b h u^2$

where C_D is the drag coefficient, ρ is the fluid density, b is the breadth of the debris dam transverse to the flow direction, h is the flow depth, and u is the flow velocity. For bridge piers, C_D is generally taken as 1.4, corresponding to a square-ended pier. In the FEMA P646 Guidelines for the Design for Vertical Evacuation from Tsunamis (FEMA, 2012), to conservatively estimate the hydrodynamic loads, a C_D value of 2.0 for tsunami events was recommended.

The recommended breadth of the debris dam has a variety of definitions. The Canadian Bridge Design Guidelines (CSA, 2006) suggests a breadth equal to that of the bridge pier. The FEMA P646 (2012) recommends a minimum breadth equal to the largest length of the available debris at the site. The ASCE7 Chapter 6 (Chock, 2016) considers any structure, regardless of mitigating breakaway walls, should consider a minimum blockage of 50% for an at-risk exposed section. Field surveys have noted the site-specific nature of debris dam formation (Parola, 2000) and therefore, where possible, site evaluations are recommended across the various standards.

While debris damming has been observed in many extreme flooding events, such as the 2005 Hurricane Katrina, 2006 Switzerland Flood, and the 2010 Chilean Tsunami (Robertson et al., 2007; Schmocker et al., 2011; Takahashi et al., 2010), the study of debris damming has primarily been performed within the context of river engineering. Bocchiola et al., (2006) examined the spatial distribution of debris damming through randomly placed obstacles. The study found that the amount of debris captured increased with the length of the debris and decreased with the flow velocity. Increased length of the debris resulted in the debris being more often captured by a “bridging” mechanism, where the debris would be caught on multiple obstacles. The “bridging” was more stable than the alternative “leaning” mechanism, where the debris would be captured on a single obstacle. Therefore “bridging” was considered more likely to form a debris dam. Similarly, the higher flow velocities resulted in less stable capture of the debris resulting in the accumulation being washed away prior to a stable dam being formed. In this work, a “debris dam” will refer to a stable formation of debris accumulation and “debris accumulation” will refer to the transient features of debris advected within a flow.

A thorough review of debris damming literature leads to the conclusion that the examination of debris damming has been predominantly performed in *steady-state subcritical* flow conditions. However, many flooding events, particularly tsunamis and flash-floods, have *transient* flow properties (Ghobarah et al., 2006; Ioualalen et al., 2007; Saatcioglu et al., 2005) and can enter into trans-critical/supercritical (*Fr* > 1) flow regimes (Fritz et al., 2006; Matsutomi et al., 2010; Titov et al., 1997). Previous research into the hydraulic loads and flow-structure interaction associated with unsteady tsunami-like waves has shown distinctive wave profiles of transient nature that significantly differ from steady-state conditions (Arnason et al., 2009; Goseberg et al., 2014; St-Germain et al., 2013). Therefore, this study examines the formation and loading conditions associated with a debris dam in unsteady supercritical flow conditions with the objectives of:

- Studying the formation of debris dams in unsteady flow conditions.
- Contrast the transient dam formation to the formation mechanisms described by Schmocker et al., (2013).
- Examining the influence of debris shape on the formation and stability of the debris dam.
- Evaluating the loading conditions on the obstacle as a result of the debris dam formation.

This paper is separated into the following sections: “Methodology” details the facilities and instrumentation used in this study as well as the experimental protocol; “Results” details the key results of the study

emphasizing the above stated objectives of the paper; “Discussion” describes key findings in the context of the wider research and discusses potential scale effects; “Conclusions” outlines the results of this study and identifies key conclusions related to the objectives.

2 METHODOLOGY

2.1 Facilities

The experiments were performed in the High-Discharge Flume at Waseda University, Tokyo (Japan). The flume shown in Figure 1 was 14.0 m long x 0.40 m wide x 0.80 m high. The flume was separated into two sections: the reservoir (light blue) and the propagation section. The floor of both sections was stainless steel. The propagation section consisted of a 2.0 m long 1:10 slope followed by a 4.0 m flat section. The 1:10 slope was used to provide adequate storage from the high-discharge flow to avoid any backwater effects caused by the flow exceeding the outlet capacity. Rapid opening of a partial lift gate resulted in a dam-break wave which propagated along the flume axis as a hydraulic bore (Chanson, 2006). A full description of the lift gate can be found in Esteban et al., (2017). The debris used in this study were scaled-down versions of common coastal debris: shipping containers (SC), hydro poles (HP), and damaged drywall panels (referred to herein as boards) (B). The debris (discussed further in Section 2.2) were placed 1.0 m from the edge of the slope downstream to allow for adequate time for the bore to develop once it had passed the sloped section.

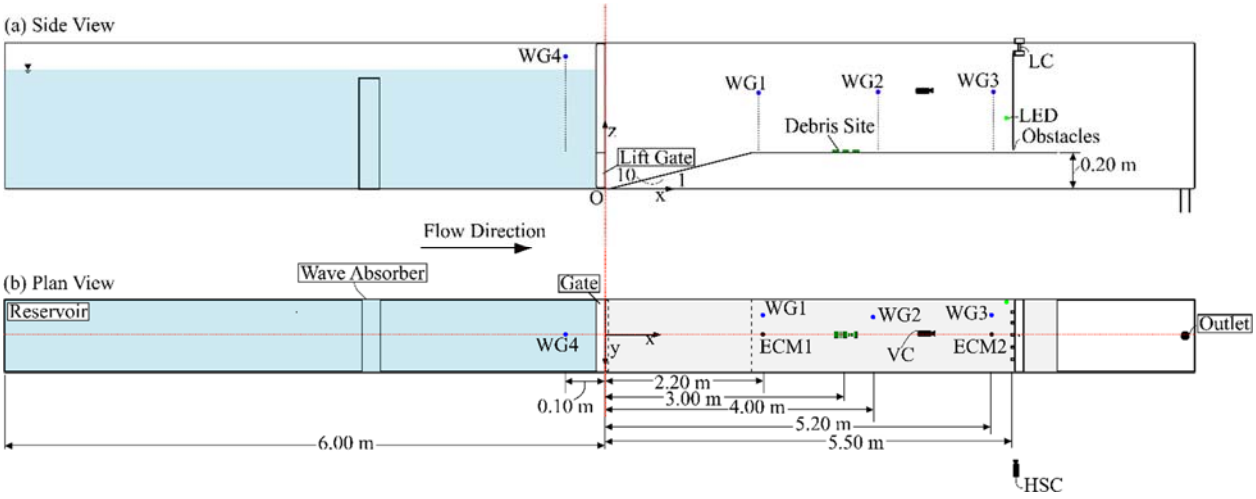

Figure 1. High-Discharge Flume at Waseda University, Tokyo. Blue dots indicate the position of a wave gauge (WG); black dots represent a position of the electromagnetic current meter (ECM).

The obstacles to be impacted by the debris were modelled as a set of columns using a 1:50 length scale and placed 5.50 m downstream from the gate. The obstacles were modelled after structural columns in a building where breakaway walls had previously been destroyed by the inundating flow. The width of the columns was chosen based on the general office prescriptions from the National Building Code of Canada (2005). The columns were 0.014 m wide with an opening width (W) of 0.06 m between each of the obstacles. The gap between the obstacles and the flume wall were 0.04 m on both sides. The obstacles were 0.40 m high. The obstacles were placed 0.005 m above the bed surface to prevent them from touching the bed surface and thus biasing the force measurements from the load cell (LC).

Table 1 lists the instrumentation used in this experiment. The positions of the instruments are shown in Figure 1. Wave gauge (WG) 4, placed in the reservoir section, was used as the reference WG for each of the experimental trials. For the remainder of this study, time = 0.00 s (zero time) refers to the time where the water depth at WG4 drops 0.002 m. The instrumentation placed downstream of the debris site (except the video camera (VC)) was removed for the cases where debris was present to avoid accidental damage. The VC and high-speed camera (HSC) were used to monitor the evolution of the debris dam. To

synchronize the cameras with the hydrodynamic data, a LED was placed in the field-of-vision of both cameras. An algorithm was written post-processing to monitor the LED and the time within the video file when the LED turned on could be determined. When the LED turned on, the voltage would be recorded by the data acquisition system (DAQ) to have a reference time between the hydrodynamics recorded by the DAQ and the video files from the cameras.

Table 1. Experimental Instrumentation.

Instrumentation	Model	Instruments	Sampling Rate
Wave Gauge (WG)	KENEK CH-601	WG1, WG2, WG3	100 Hz
Electro-current Meter (ECM)	KENEK MT2-200	ECM1, ECM2	100 Hz
Video Camera (VC)	JVC Everio GZ-HM440		60 FPS
High-Speed Camera (HSC)	KATO KOKEN k4		100 FPS
Load Cell (LC)	SSK LB120-50		100 Hz

2.2 Debris

The experiments were performed considering Froude similitude (1:50 geometric length scale). Three different types of debris were selected based on the debris indicated in the ASCE7 Chapter 6 (Chock, 2016) and the FEMA P646 (FEMA, 2012) (Figure 2). All the debris were built from pine wood (specific gravity (SG) = 0.47) and were therefore positively buoyant. The shipping containers (SC) were modelled as an International Organization of Standardization (ISO) 6.1 m shipping container (0.12 m x 0.045 m x 0.045 m) (Goseberg et al., 2016; Nistor et al., 2016; Stolle et al., 2016). The hydro poles (HP) were modelled as standard 6.1 m hydro poles (0.12 m x 0.005 m diameter). The board (B) was designed considering an arbitrary shape of a piece of drywall washed away from another structure (0.06 m x 0.04 m x 0.002 m). Each debris was weighed for an average weight of 0.111 kg (prototype scale = 13 875 kg), 0.002 kg (250 kg), and 0.004 kg (500 kg) for the SC, B, and HP, respectively. The standard deviation of the weight between debris was 0.001 kg.

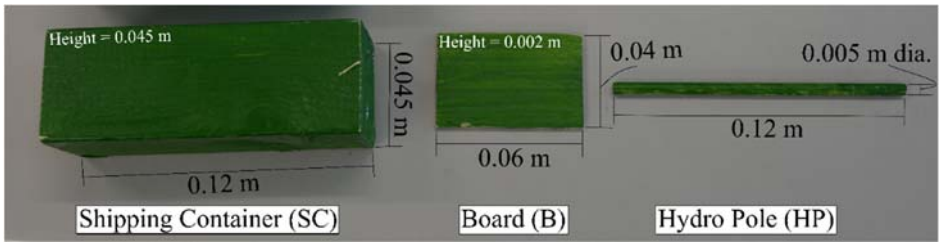

Figure 2. Type of debris modelling in tsunami-like conditions: Shipping containers (SC), board (B), and hydro poles (HP)

2.3 Experimental Protocol

The experiments can be separated into three categories: same volume cases (SV), same plan area cases (PA), and the debris mixture cases (DM). An additional set of tests were performed to examine the repeatability of the hydrodynamics with nod debris and without (no obstacles) the structure. The same volume cases (equally combined volume of all debris in a test) were performed to examine the influence of the individual debris properties on the capture efficiency and associated loads. The plan area experiments refer to the plan area of the debris when observing the debris from a top view. The ASCE7 Chapter 6 assessment of debris impact potential relies upon the plan area of the debris (Chock, 2016; Naito et al., 2014; Naito et al., 2016), therefore the amount of debris in the same plan area category was selected based on the plan area. The debris mixtures were selected to examine the influence of the debris types in

combination on the dam formation. For each category, the experiments were performed with three different impoundment water depths: 0.40 m, 0.50 m, and 0.60 m. Each experiment was performed with 3 repetitions for a total of 125 experimental trials.

Table 2. Experimental Protocol.

Impoundment Water Depth [m]	Debris Mixture [SC, HP, B]	Experimental Category
0.4	0,0,0	
0.5	9,0,0	PA
0.6	0,81,0	PA
	0,0,20	PA
	3,27,7	PA/DM
	7,9,2	PA/DM
	1,63,2	PA/DM
	1,9,16	PA/DM
	6,54,14	DM
	9,81,20	DM
	1,0,0	SV
	0,103,0	SV
	0,0,51	SV

3 RESULTS

3.1 Hydrodynamics

Figure 3 shows the clear-water (no debris) conditions at the obstacles position. Figure 3a-b show the water depth and the flow velocity at the obstacle site (WG3 and ECM2). The wave front velocities at the obstacle site are plotted as open diamonds in Figure 3b. These were estimated using the difference in the wave arrival time between WG2 and WG3. Flow velocities were measured using ECM2; however, due to air entrainment and cavitation occurring in the initial wave front, data could not be accurately captured for the first ~2 s of the wave front.

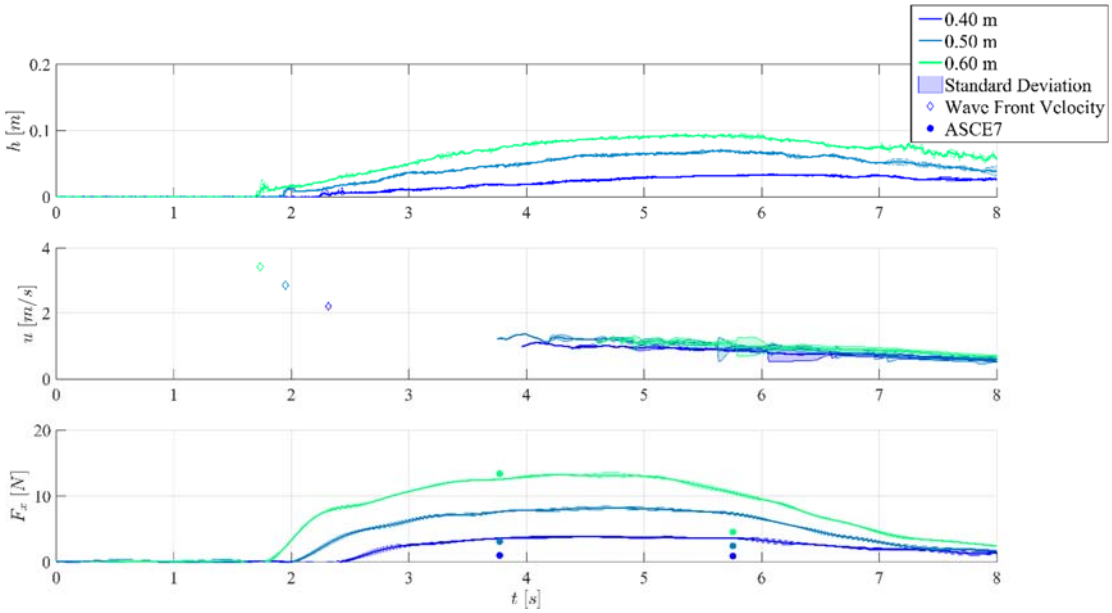

Figure 3. Hydrodynamic conditions at the site of the obstacle (no debris case). The water surface elevation and flow velocity taken with the obstacles in place. The filled circular markers represent the calculated drag forces from the ASCE7 Chapter 6.

The clear-water force profile in the flow direction (Figure 3c) was measured with the LC connected to the obstacles. The force profiles are compared to the ASCE7 standard (Eq. 1) at the point of 2/3 the wave front velocity and the maximum water depth (filled circles). These two time instances were chosen based on the critical design loads outlined in the ASCE7 standard (Chock, 2016). Generally, the ASCE7 standard overpredicted the hydrodynamic forces for the clear-water case. The Froude number from field investigations of tsunami events have ranged from 0.6 – 1.4 (Fritz et al., 2006; Fritz et al., 2012; Matsutomi et al., 2010). The Froude number in these experiments ranged from 1.2 – 1.9, exceeding the expected range in a tsunami-like event. Bricker et al., (2015) in an examination of Manning's *n* values used in tsunami modelling, emphasized the necessity of properly scaling experiments, particularly related to the Reynolds (Re) and Weber (We) numbers. The Re and We number were calculated at the point where the ECM first recorded consistent velocity values. Te Chow, (1959) noted that flow conditions should be fully turbulent ($Re > 1.25x10^4$) and Peakall et al., (1996) indicated that We > 120 - both of these conditions are achieved in these experiments.

3.2 Debris Dam Formation

The formation of a debris dam in steady-state subcritical flow conditions has been well-established by Schmocker et al., (2013). According to these authors, the debris initially passed through the obstacles until the first debris was caught in the obstacle, commonly referred to as the "key log." Once the "key log" had formed, the debris were pushed by the streamlines surrounding the "key log" to fill the width of the obstacle. As the width was filled, the debris would begin to compact those at the front of the structure, forcing them towards the bed and obstructing thus the channel cross-section. As a result, the water depth upstream of the dam began to rise and the flow velocity decreased. Once the flow velocity had decreased, compaction no longer occurred and a debris carpet on the water surface begun forming upstream of the obstacle. The extent of each of these steps could be dependent on the flume dimensions and initial flow conditions. Equivalently, the companion study to the work performed here (Stolle et al., 2017) with the same debris under steady-state flown conditions displayed a similar behavior.

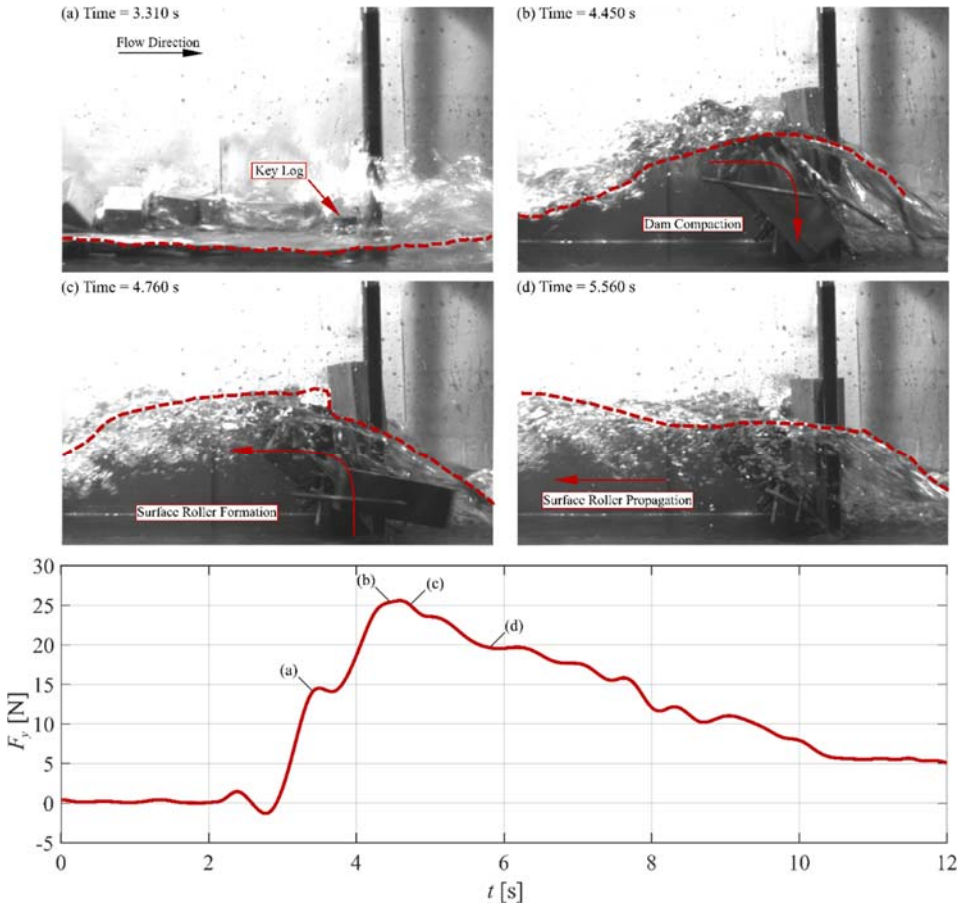

Figure 4. Debris dam formation for the case with 9 SC, 81 HP, 20 B and 0.40 m impoundment depth. Panels (a)-(d) show still images from the HS at various key point. The red dashed line is marking the water surface elevation. Panel (e) shows the force-time history for the experiment, the times corresponding to the above images are indicated within the figure.

Figure 4 shows the formation of the debris dam in unsteady supercritical flow conditions. Due to the supercritical flow conditions and the high velocity flow, stream lines did not fully form (Soares-Frazão et al., 2007) and debris were not pushed to obstruct the full width of the obstacle. Unlike the steady-state cases where the stagnation zone had adequate time to form before the debris arrived. The transient flow case instead, caused by the high-velocity flow, moved into the rapid compaction of the dam causing a constriction of the cross-section. As the constriction formed, the water would runup the structure formed a surface roller directly upstream of the structure (Figure 4b), similar to the surface piercing columns in dam-break flows (St-Germain et al., 2013). Due to the supercritical flow conditions, the rise in water surface level did not propagate upstream as was observed in the steady-state case. Instead, the surface roller expanded in cross-stream direction until it reached the walls of the flume; at that point, the surface roller propagated upstream. St-Germain et al., (2013) also noted that this was the point of maximum runup. Similarly, the maximum force and runup corresponded with the instant just before the surface roller began to propagate back upstream (Figure 4e). The vortices formed by the surface roller destabilised the dam formation causing its constituting parts to break apart and be washed downstream, past the obstacles (Figure 4c). As the surface roller propagated upstream, the reduction of flow velocity and return of predominantly unidirectional flow resulted in the dam stabilizing (Figure 4d).

3.3 Debris Dam Loading

In Equation 1, the drag coefficient (C_D) was used to calculate the drag force acting on a structure. However, the classical definition of the drag coefficient refers to the case when the obstacle is fully submerged in the

flow (Qi et al., 2014). In the experiments presented here, due to the unsteady, energetic nature of the flow, a wake formed behind the structure resulting in an unbalanced hydrostatic force acting on the structure (**Error! Reference source not found.**). As such, the drag coefficient cannot be determined within this study. Arnason et al., (2009), in a study of bore impingement on a vertical column, instead used a similar resistance coefficient (C_R) which manifests as a time history due to the fluctuation in the hydrostatic component.

[2] $C_R = \frac{2F_x}{\rho h b u^2}$

The resistance coefficient C_R was taken as mean resistance coefficient in the first 5 seconds after the wave arrival to avoid any influence from the reservoir. The characteristic length used in the calculation of the Fr_d and Re_d was the dam width at the time of occurrence of the maximum force. Due to the unsteady conditions and formation of the surface roller, a reference unperturbed upstream state could not be achieved. Therefore, the velocity and water depth used in the calculation of C_R was taken from the clear-water condition (Bremm et al., 2015) at the same instant. A log-log transformation was applied to the dataset to achieve an approximately linear regression (R^2 = 0.821). The resulting coefficients of the regression were a = 3.58 x 10^5 and b = -1.089. The focus of this study addressed the forces in supercritical flow conditions: it is therefore unclear if the same trend could be extended to subcritical flow conditions, rendering thus necessary future research on transient subcritical conditions.

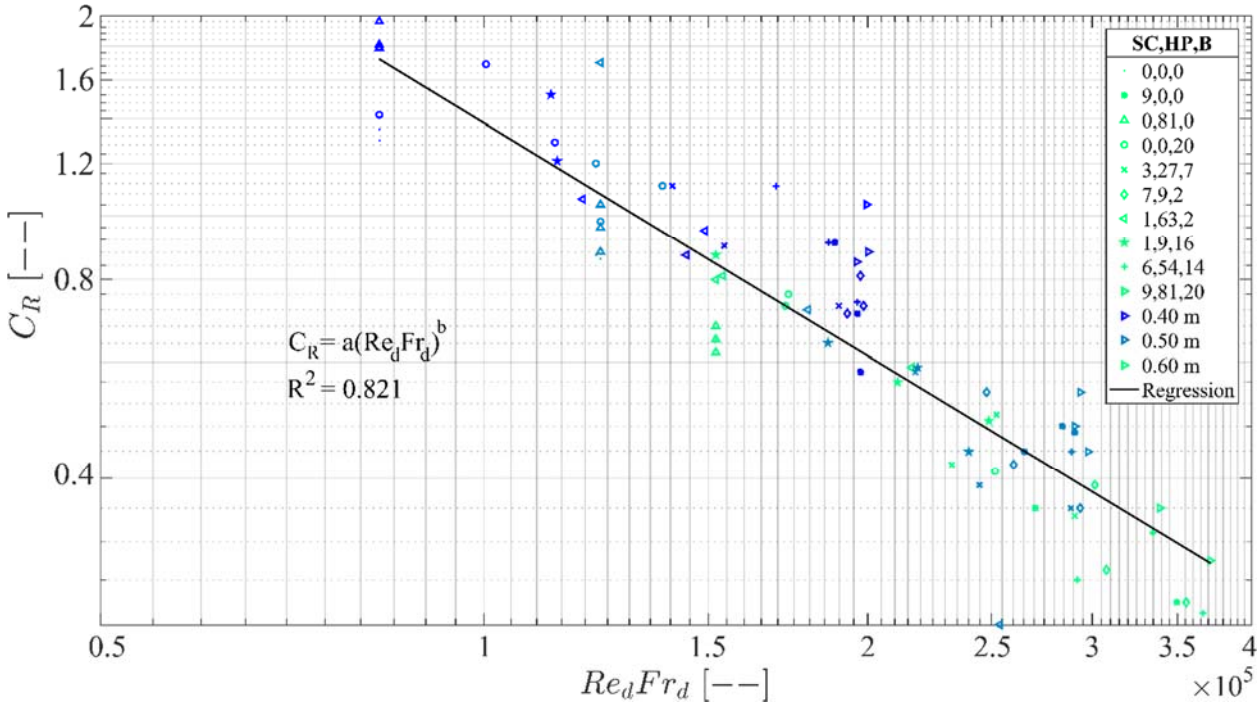

Figure 5. Resistance coefficient, C_R as a function of the product of the Reynolds and Froude number. The different debris mixtures are indicated by the marker type and the initial impoundment depth by the marker color. The log-log regression line is displayed as a solid black line.

4 CONCLUSIONS

The study discussed herein examined the formation and loads associated with debris dams in supercritical, unsteady flow conditions. The study focused on the debris damming in a coastal setting by modelling debris common to a coastal environment and by using a hydrodynamic forcing condition similar to a tsunami wave. The paper investigated the influence of the debris mixtures on the size of the debris dam, the runup at the structure face, and the loads exerted on the structure.

Based on the results, the following conclusions can be drawn:

- The debris dam formation was initiated similarly to the steady-state cases, as described in Schmocker et al. (2013). However, due to the supercritical flow conditions, a debris carpet was not formed in front of the dam.
- Due to the formation of the surface roller at the structure face, the dam would break apart as the surface roller propagated upstream, resulting in the dam being less stable than the unidirectional cases.
- The resistance coefficient showed an approximately log-log linear relationship with the product of the Reynolds and Froude number.

Debris damming has been shown to be a major concern in flooding events, and therefore needs to be carefully considered in the design process of infrastructure exposed to such effects. The study presented herein was the first to examine debris damming in unsteady flow conditions. Based on climate change studies on precipitation patters, intensity and possibly frequency of transient flows will likely increase; hence, designing for such extreme flows is of major interest for engineers. However, due to concerns of damage to instrumentation in such conditions, research is further needed into the changing hydrodynamic conditions around the debris dam formation. While the focus of this experimental program was modelling tsunami-like flow conditions, the general conclusions of this study can be applied to rapidly occurring flooding events, such as flash floods and flood waves from breaching dams, where supercritical flow are present.

Acknowledgements

The authors are acknowledging the support of the NSERC CGS-D Scholarship (Jacob Stolle), of the NSERC Discovery Grant (No. 210282) (Ioan Nistor), the Marie Curie International Outgoing Fellowship within the 7th European Community Framework Program (No. 622214) (Nils Goseberg), and the Strategic Research Foundation Grant-aided Project for Private Universities from the Japanese Ministry of Education, Culture, Sports, Science and Technology (No. S1311028) (Tomoya Shibayama). The authors would also like to acknowledge the help of the Waseda University technical staff in the design and implementation of the experimental setup, in particular Mr. Kazuhiro Yamanashi, Mr. Kiyoji Egawa, and Mr. Akihiro Kagami.

References

AASHTO 2012. Bridge design specifications.

Arnason, H., Petroff, C. & Yeh, H. 2009. Tsunami bore impingement onto a vertical column. Journal of Disaster Research 4(6), 391–403.

Bocchiola, D., Rulli, M. & Rosso, R. 2006. Transport of large woody debris in the presence of obstacles. Geomorphology 76(1), 166–178.

Bremm, G.C., Goseberg, N., Schlurmann, T. & Nistor, I. 2015. Long Wave Flow Interaction with a Single Square Structure on a Sloping Beach. Journal of Marine Science and Engineering 3(3), 821.

Bricker, J.D., Gibson, S., Takagi, H. & Imamura, F. 2015. On the need for larger Manning's roughness coefficients in depth-integrated tsunami inundation models. Coastal Engineering Journal 57(02), 1550005.

Chanson, H. 2006. Tsunami surges on dry coastal plains: Application of dam break wave equations. Coastal Engineering Journal 48(04), 355–370.

Chock, G.Y. 2016. Design for tsunami loads and effects in the ASCE 7-16 standard. Journal of Structural Engineering, 04016093.

CREW 2013. Cascadia subduction zone earthquakes: A magnitude 9.0 earthquake scenario, Oregon Department of Geology and Mineral Industries,p.

CSA 2006. Canadian highway bridge design code, CSA,p.

Esteban, M., Takagi, H. & Shibayama, T. 2015. Handbook of Coastal Disaster Mitigation for Engineers and Planners.

Esteban, M., Glasbergen, T., Takabatake, T., Hofland, B., Nishizaki, S., Nishida, Y., Stolle, J., Nistor, I., Bricker, J., Takagi, H. & others 2017. Overtopping of Coastal Structures by Tsunami Waves. Geosciences 7(4), 121.
FEMA 2012. P646 Guidelines for Design of Structure for Vertical Evacuation from Tsunamis. Federal Emergency Management Agency.
Fritz, H.M., Borrero, J.C., Synolakis, C.E. & Yoo, J. 2006. 2004 Indian Ocean tsunami flow velocity measurements from survivor videos. Geophysical Research Letters 33(24).
Fritz, H.M., Phillips, D.A., Okayasu, A., Shimozono, T., Liu, H., Mohammed, F., Skanavis, V., Synolakis, C.E. & Takahashi, T. 2012. The 2011 Japan tsunami current velocity measurements from survivor videos at Kesennuma Bay using LiDAR. Geophysical Research Letters 39(7).
Ghobarah, A., Saatcioglu, M. & Nistor, I. 2006. The impact of the 26 December 2004 earthquake and tsunami on structures and infrastructure. Engineering structures 28(2), 312–326.
Goseberg, N. & Schlurmann, T. 2014. Non-stationary flow around buildings during run-up of tsunami waves on a plain beach. Coastal Engineering Proceedings 1(34), 21.
Goseberg, N., Stolle, J., Nistor, I. & Shibayama, T. 2016. Experimental analysis of debris motion due the obstruction from fixed obstacles in tsunami-like flow conditions. Coastal Engineering 118, 35–49.
Ioualalen, M., Asavanant, J., Kaewbanjak, N., Grilli, S., Kirby, J. & Watts, P. 2007. Modeling the 26 December 2004 Indian Ocean tsunami: Case study of impact in Thailand. Journal of Geophysical Research: Oceans (1978–2012) 112(C7).
Matsutomi, H. & Okamoto, K. 2010. Inundation flow velocity of tsunami on land. Island Arc 19(3), 443–457.
Naito, C., Cercone, C., Riggs, H.R. & Cox, D. 2014. Procedure for site assessment of the potential for tsunami debris impact. Journal of Waterway, Port, Coastal and Ocean Engineering 140(2), 223–232.
Naito, C., Riggs, H., Wei, Y. & Cercone, C. 2016. Shipping-Container Impact Assessment for Tsunamis. Journal of Waterway, Port, Coastal, and Ocean Engineering, 05016003.
Nistor, I., Goseberg, N., Mikami, T., Shibayama, T., Stolle, J., Nakamura, R. & Matsuba, S. 2016. Hydraulic Experiments on Debris Dynamics over a Horizontal Plane. Journal of Waterway, Port, Coastal and Ocean Engineering, 04016022.
Parola, A.C. 2000. Debris forces on highway bridges, Transportation Research Board,p.
Peakall, J. & Warburton, J. 1996. Surface tension in small hydraulic river models-the significance of the Weber number. Journal of Hydrology New Zealand 35, 199–212.
Qi, Z., Eames, I. & Johnson, E. 2014. Force acting on a square cylinder fixed in a free-surface channel flow. Journal of Fluid Mechanics 756, 716–727.
Robertson, I., Riggs, H.R., Yim, S.C. & Young, Y.L. 2007. Lessons from Hurricane Katrina storm surge on bridges and buildings. Journal of Waterway, Port, Coastal, and Ocean Engineering 133(6), 463–483.
Saatcioglu, M., Ghobarah, A. & Nistor, I. 2005. Effects of the December 26, 2004 Sumatra earthquake and tsunami on physical infrastructure. ISET Journal of earthquake technology 42(4), 79–94.
Schmocker, L. & Hager, W.H. 2011. Probability of drift blockage at bridge decks. Journal of Hydraulic Engineering 137(4), 470–479.
Schmocker, L. & Hager, W.H. 2013. Scale modeling of wooden debris accumulation at a debris rack. Journal of Hydraulic Engineering 139(8), 827–836.
Soares-Frazão, S. & Zech, Y. 2007. Experimental study of dam-break flow against an isolated obstacle. Journal of Hydraulic Research 45(sup1), 27–36.
St-Germain, P., Nistor, I., Townsend, R. & Shibayama, T. 2013. Smoothed-particle hydrodynamics numerical modeling of structures impacted by tsunami bores. Journal of Waterway, Port, Coastal, and Ocean Engineering.
Stolle, J., Nistor, I. & Goseberg, N. 2016. Optical Tracking of Floating Shipping Containers in a High-Velocity Flow. Coastal Engineering Journal, 1650005.
Stolle, J., Takabatake, T., Mikami, T., Shibayama, T., Goseberg, N., Nistor, I. & Petriu, E. 2017. Experimental Investigation of Debris-Induced Loading in Tsunami-Like Flood Events. Geosciences 7, 74.
Takahashi, S., Sugano, T., Tomita, T., Arikawa, T., Tatsumi, D., Kashima, H., Murata, S., Matsuoka, Y. & Nakamura, T. 2010. Joint survey for 2010 Chilean earthquake and tsunami disaster in ports and coasts. Port and Airport Res Inst.
Te Chow, V. 1959. Open channel hydraulics, McGraw-Hill Book Company, Inc; New York,p.

Titov, V.V. & Synolakis, C.E. 1997. Extreme inundation flows during the Hokkaido-Nansei-Oki tsunami. Geophysical Research Letters 24(11), 1315–1318.
Yeh, H., Sato, S. & Tajima, Y. 2013. The 11 March 2011 East Japan earthquake and tsunami: tsunami effects on coastal infrastructure and buildings. Pure and Applied Geophysics 170(6-8), 1019–1031.
Yeh, H., Barbosa, A.R., Ko, H. & Cawley, J.G. 2014. Tsunami Loadings on Structures: Review and Analysis. Coastal Engineering Proceedings 1(34), currents–4.